The small G-protein MglA connects to the MreB actin cytoskeleton at bacterial focal adhesions

Anke Treuner-Lange,[1]* Eric Macia,[2]* Mathilde Guzzo,[3]* Edina Hot,[1]* Laura M. Faure,[3] Beata Jakobczak,[1] Leon Espinosa,[3] Damien Alcor,[2] Adrien Ducret,[3] Daniela Keilberg,[1] Jean Philippe Castaing,[3] Sandra Lacas Gervais,[4] Michel Franco,[2] Lotte Søgaard-Andersen,[1] and Tâm Mignot[3]

[1]Max Planck Institute for Terrestrial Microbiology, 35043 Marburg, Germany
[2]Institut de Pharmacologie Moléculaire et Cellulaire, UMR 7275 Centre National de la Recherche Scientifique, Université de Nice Sophia Antipolis, 06560 Valbonne, France
[3]Laboratoire de Chimie Bactérienne, UMR 7283 Centre National de la Recherche Scientifique, Aix Marseille University, 13009 Marseille, France
[4]Centre Commun de Microscopie Appliquée, Université de Nice Sophia Antipolis, 06103 Nice, France

In *Myxococcus xanthus* the gliding motility machinery is assembled at the leading cell pole to form focal adhesions, translocated rearward to propel the cell, and disassembled at the lagging pole. We show that MglA, a Ras-like small G-protein, is an integral part of this machinery. In this function, MglA stimulates the assembly of the motility complex by directly connecting it to the MreB actin cytoskeleton. Because the nucleotide state of MglA is regulated spatially and MglA only binds MreB in the guanosine triphosphate–bound form, the motility complexes are assembled at the leading pole and dispersed at the lagging pole where the guanosine triphosphatase activating protein MglB disrupts the MglA–MreB interaction. Thus, MglA acts as a nucleotide-dependent molecular switch to regulate the motility machinery spatially. The function of MreB in motility is independent of its function in peptidoglycan synthesis, representing a coopted function. Our findings highlight a new function for the MreB cytoskeleton and suggest that G-protein–cytoskeleton interactions are a universally conserved feature.

Introduction

Regulated cell motility drives many physiological processes including organ formation during embryogenesis, wound healing, the onset of the immune response, and cancer metastasis in metazoans (Charest and Firtel, 2007). In bacteria, cell motility is essential for the colonization of diverse habitats as well as for the formation of higher-order structures such as biofilms and fruiting bodies (Harshey, 2003). In eukaryotic cells, motility generally depends on the dynamic reorganization of the actin cytoskeleton and is powered at so-called focal adhesions (FAs) that form at the leading cell edge and disassemble at the rear edge, allowing cells to move over long distances (Heasman and Ridley, 2008). Although, the molecular composition of FAs varies between cell types, in all cases the formation of FAs regroups the actomyosin cytoskeleton to establish an adhesive complex, allowing the transduction of traction forces to the underlying substratum. Motility is highly regulated and, consistently, FAs incorporate regulators that govern the activity and assembly/disassembly of FAs. Among these regulators, small G-proteins of the Ras superfamily are vastly used and function as nucleotide-dependent molecular switches that interact with cognate effectors when bound to GTP.

Bacteria move on surfaces using flagella or type IV pili or by gliding (Jarrell and McBride, 2008). Although flagella- and type IV pili–based motilities are well understood, gliding motility, which occurs in the absence of extracellular organelles, is poorly understood mechanistically. Recent work on the rod-shaped cells of *Myxococcus xanthus* has started to uncover the gliding motility mechanism. *M. xanthus* cells move by gliding motility in the direction of their long axis and, thus, have a leading and a lagging cell pole (Zhang et al., 2012a). Gliding motility is powered by the recently characterized Agl–Glt complex, a macromolecular system thought to be formed by at least 14 proteins composed of two subcomplexes: the motor subcomplex (Agl), a proton-conducting channel homologous to the motor that drives rotation of bacterial flagella consisting of the three inner membrane proteins AglR, Q, and S (Sun et al., 2011; Nan et al., 2013;

*A. Treuner-Lange, E. Macia, M. Guzzo, and E. Hot contributed equally to this paper.

Correspondence to Michel Franco: franco@ipmc.cnrs.fr; Lotte Søgaard-Andersen: sogaard@mpi-marburg.mpg.de; or Tâm Mignot: tmignot@imm.cnrs.fr

A. Ducret's present address is Dept. of Biology, Indiana University, Bloomington, IN 47405.

Abbreviations used in this paper: DLS, dynamic light scattering; FA, focal adhesion; GAP, GTPase activating protein; MIC, minimum inhibitory concentration; PG, peptidoglycan; WT, wild type.

The Rockefeller University Press $30.00
J. Cell Biol. Vol. 210 No. 2 243–256
www.jcb.org/cgi/doi/10.1083/jcb.201412047

Balagam et al., 2014); and the Glt subcomplex, which has been suggested to consist of 11 proteins (GltA-K) predicted to localize in different cell envelope compartments including the cytoplasm, inner membrane, periplasm, and outer membrane (Fig. 1; Nan et al., 2010; Luciano et al., 2011; Sun et al., 2011). The Agl and Glt subcomplexes are suggested to associate via a direct interaction involving AglR and GltG (Luciano et al., 2011). The propulsion mechanism has been partially characterized: after its assembly at the leading pole, the Agl–Glt complex moves directionally along an as yet unidentified seemingly helical track powered by the Agl motor directly and the proton motive force (Fig. 1; Sun et al., 2011; Nan et al., 2013; Balagam et al., 2014). Thrust is thought to occur when the combined Agl–Glt motility machinery contacts and adheres to the underlying substratum forming on average three to four bacterial FA-like complexes per cell that are regularly distributed along the cell (Fig. 1). In a motile cell, these bacterial FA complexes retain fixed positions relative to the underlying surface until they become disassembled at the lagging pole, in this way allowing a cell to move over long distances (Fig. 1; Mignot et al., 2007). Thus, there must be mechanisms that control Agl–Glt assembly at the leading cell pole and its dispersal at the lagging cell pole. Additional proteins (AglZ and MglA) also localize to FAs (Fig. 1) and we show here that they are involved in the spatial regulation of the motility complex.

Three proteins have enigmatic functions in gliding motility in *M. xanthus*, the small Ras-like G-protein MglA, the coiled-coil protein AglZ, and the actin homologue MreB. MglA is absolutely required for gliding in *M. xanthus* (Hodgkin and Kaiser, 1979) and functions as a nucleotide-dependent molecular switch to stimulate motility (Mauriello et al., 2010; Leonardy et al., 2010; Patryn et al., 2010; Zhang et al., 2010; Miertzschke et al., 2011). As most proteins of the Ras superfamily of small G-proteins, MglA is active in its GTP-bound state and inactive in the GDP-bound state (Leonardy et al., 2010; Zhang et al., 2010; Miertzschke et al., 2011). GTP hydrolysis by MglA is stimulated by MglB, a GTPase activating protein (GAP; Leonardy et al., 2010; Zhang et al., 2010; Miertzschke et al., 2011), whereas a guanine nucleotide exchange factor has not been identified. MglA-GTP accumulates at the leading cell pole, whereas MglA-GDP is diffusely localized in the cytoplasm (Leonardy et al., 2010; Patryn et al., 2010; Zhang et al., 2010). MglB localizes to the lagging cell pole (Leonardy et al., 2010; Zhang et al., 2010; Miertzschke et al., 2011). MglB excludes MglA-GTP from the lagging pole by converting MglA-GTP to MglA-GDP and, thus, sets up the MglA-GTP asymmetry (Leonardy et al., 2010; Zhang et al., 2010, 2012b; Keilberg et al., 2012). MglA has also been suggested to localize to distributed fixed clusters in motile cells and regulate the directionality of the Agl motor through interactions with AglZ and AglR, a motor component, indicating that MglA could be an integral part of FAs (Yang et al., 2004; Patryn et al., 2010; Mauriello et al., 2010; Nan et al., 2015). However, how these interactions relate to motility and how MglA-GTP stimulates gliding motility is currently unknown. The actin homologue MreB, which is important for peptidoglycan (PG) cell wall synthesis in rod-shaped bacteria (Typas et al., 2012; Errington, 2015), is also important for gliding motility, i.e., chemical interference with MreB polymerization by the compound A22 blocks gliding as well as AglZ localization to FAs (Mauriello et al., 2010).

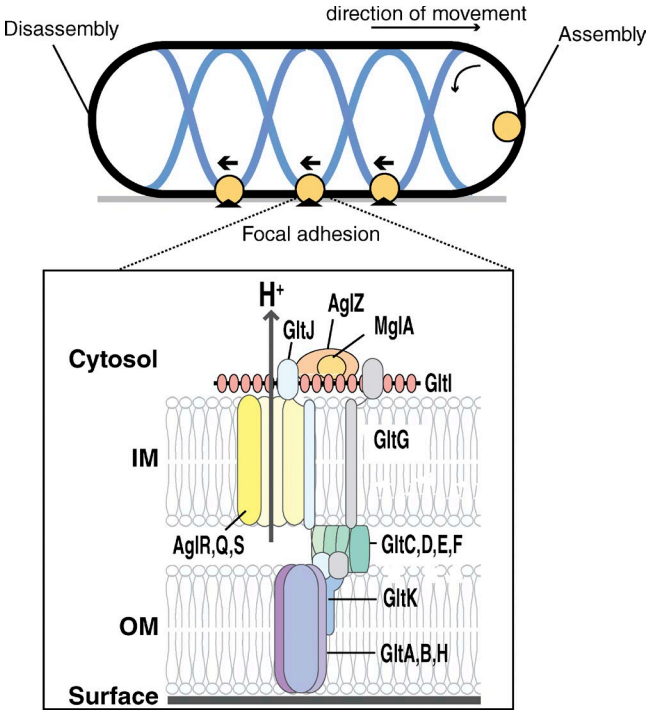

Figure 1. **The *M. xanthus* motility machinery.** The current model proposes that the motility complex (yellow circle) is assembled at the leading cell pole and traffics toward the lagging cell pole along a hypothetical looped track (blue). Immobilization at bacterial FAs converts this movement into propelling forces. Active complexes are disassembled when they reach the lagging cell pole while new complexes are formed at the leading cell pole, allowing persistent directional movements. A proposed architecture of the complex is shown. Protein domains and their localization are inferred from sequence prediction and experimental evidence. Proteins used in this study: AglQ (yellow) is a TolR-like protein and contains a predicted transmembrane helix, GltA (blue) has a predicted outer membrane OmpA-like fold, and GltI is a predicted giant 3,822-residue cytosolic protein containing up to 17 predicted tetratricopeptide repeat domains (pink circles). Experimental localization has been determined for AglQ, AglR, GltD, and GltF using fluorescent fusions (Luciano et al., 2011; Sun et al., 2011; Nan et al., 2011, 2013) and for GltA, D, E, F, G, and H using cell fractionation assays (Luciano et al., 2011; Jakobczak et al., 2015). The localization of GltB and GltC has not been determined for the motility system but the paralogues NfsB and NfsC have been localized by fractionation in the sporulation system (Holkenbrink et al., 2014). Direct interactions have only been shown for GltG and AglR (Luciano et al., 2011).

Interestingly, MreB also interacts directly with AglZ (Mauriello et al., 2010). How these interactions stimulate gliding motility is also currently unknown.

In this study, we investigated the function of MglA and MreB in gliding motility. We provide evidence that MglA-GTP is an integral part of the Agl–Glt gliding motility complex at FAs and stimulates the assembly of the Agl–Glt machinery at the leading pole. Moreover, we found that MreB functions in motility independently from its role in PG synthesis, interacting directly with MglA-GTP to stimulate motility complex formation. Finally, we show that breaking this interaction is essential for disassembly of the motility complexes at the lagging pole. We elucidate the mechanism and show that MglB, the cognate MglA GAP, localizes to the lagging cell pole and dissociates MglA from MreB in two additive ways: (1) MglB is competing with MreB for interaction with MglA-GTP and (2) MglB is converting MglA to the GDP-bound state, which does not interact with MreB.

Results

Localization of the Agl–Glt machinery in motile cells

To localize the Agl–Glt machinery during motility, we developed fluorescent probes to monitor the localization of three Glt proteins predicted to localize to three distinct layers of the Agl–Glt motility machinery (Fig. 1). AglQ is a subunit of the Agl motor in the inner membrane and localizes to FAs, forming multiple fixed clusters along the cell length (Sun et al., 2011). GltA is an outer membrane protein, is part of the Glt complex, and localizes to FAs (Jakobczak et al., 2015). GltI has not been previously localized but is suggested to be a component of the Agl–Glt complex (Luciano et al., 2011) and is predicted to localize in the cytosol (Fig. 1; Luciano et al., 2011). In particular, GltI lacks a predicted signal peptide. We constructed fluorescent fusions to each of these proteins to monitor their localization over time. Because in each case the fusions are expressed from their native promoters and complement deletions of the respective genes (*gltA*, *gltI*, and *aglQ* mutations all lead to nonmotile cells; Luciano et al., 2011; Sun et al., 2011), we concluded that all three fusions are functional and could be further studied. The AglQ-mCherry fusion (mCh) and GltA-mCh formed fixed clusters that became dispersed when they reached the lagging pole as previously described for AglZ-YFP (Mignot et al., 2007; Fig. 2, A and B). GltI-YFP also formed fixed clusters that became dispersed at the lagging pole (Fig. 2 C). In addition, GltA-mCh but not GltI-YFP was also localized all around the cell periphery, consistent with the localization of GltA-mCh to the outer membrane and the predicted localization of GltI-YFP to the cytosol (Fig. 2 C and Fig. S1, A and B). We conclude that GltI, AglQ, and GltA all localize to FAs in motile cells and, thus, the Agl–Glt complex likely spans the entire cell envelope (although rigorous fractionation experiments are required to formally prove the cytosolic localization of GltI).

MglA is required for the assembly and localization of the Agl–Glt machinery at FAs

Previously, MglA was shown to be important for the FA localization of AglZ-YFP (Mauriello et al., 2010). However, the exact function of the cytoplasmic AglZ protein is not known and it could be both a gliding motility regulator and a structural component of the gliding machinery (Mauriello et al., 2009, 2010). To test whether MglA is more generally important for the formation of the Agl–Glt machinery at FAs, we determined how MglA affects the localization of AglQ-mCh, GltI-YFP, and GltA-mCh. In the absence of MglA, AglQ-mCh formed a cluster at one of the cell poles in many cells but did not form clusters along the cell length (Fig. 3), whereas GltI-YFP and GltA-mCh essentially became diffusely localized in the cytosol and around the cell periphery, respectively (Figs. 3 and S1, C and D). Thus, MglA is not only required for the localization of AglZ at FAs (Mauriello et al., 2010), but most likely for the assembly and localization of the entire Agl–Glt machinery at FAs.

MglA is a component of the Agl–Glt motility machinery at FAs

MglA is active and stimulates gliding motility in its GTP-bound state and is deactivated after GTP hydrolysis. When MglA is fused to YFP, the GTP-bound form of MglA localizes predominantly to the leading cell pole and occasionally to fixed clusters along the cell length, suggesting that it can also localize to FAs

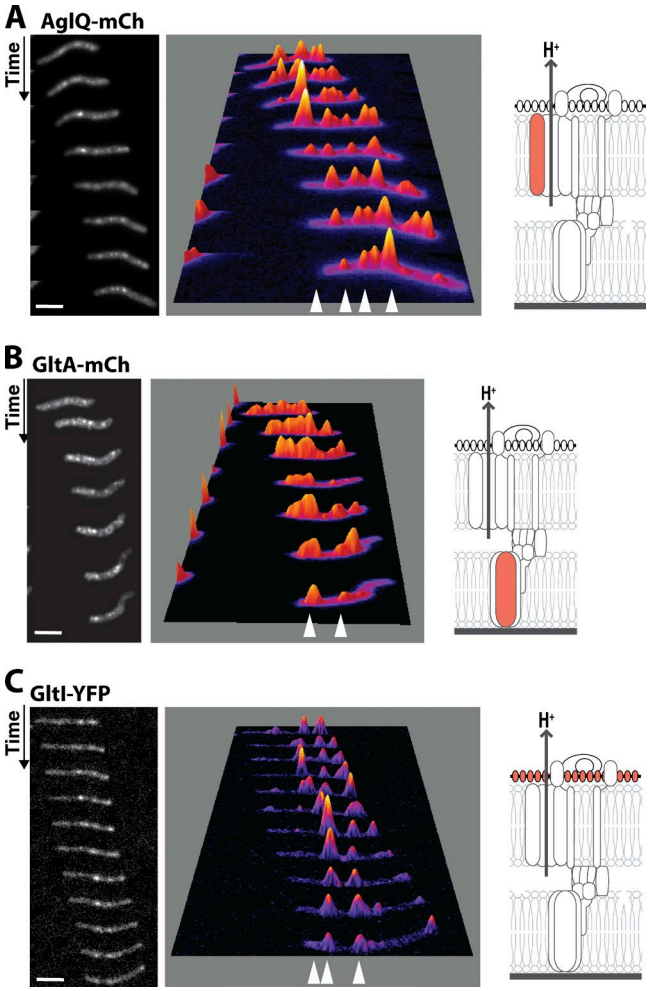

Figure 2. ***M. xanthus* FAs contain a trans-envelope complex.** Localization of AglQ-mCh (A), GltA-mCh (B), and GltI-YFP (C) in a moving WT cell. Shown are unprocessed micrographs (left) of a moving cell taken every 30 s and 3D projections of fluorescence intensities of these same micrographs. FAs (arrowheads) are apparent as intensity peaks that retain fixed positions throughout the time-lapse recordings. Bars, 2 µm. The schematic shows a model of the motility complex as in Fig. 1 and with the tagged protein indicated in light red.

(Mauriello et al., 2010; Patryn et al., 2010; Zhang et al., 2010). In wild-type (WT) cells, the regulation by GTP hydrolysis complicates the study of the function of MglA in gliding motility (Leonardy et al., 2010; Zhang et al., 2010). To circumvent this problem, we took advantage of an MglB-insensitive and constitutively activated MglA^{Q82A} variant that is locked in the GTP-bound form (Miertzschke et al., 2011). A strain expressing a YFP-MglA^{Q82A} fusion had the same motility phenotype as an MglA^{Q82A}-expressing strain and therefore the fusion was deemed functional (Miertzschke et al., 2011). In motile cells, YFP-MglA^{Q82A} localized to both cell poles and formed a single fixed fluorescent-bright cluster in motile cells as previously described (Fig. 4 A; Zhang et al., 2010; Miertzschke et al., 2011). To check if the nonpolar YFP-MglA^{Q82A} cluster reflects the assembly of a single active Agl–Glt complex, we assayed the localization of AglZ-mCh, AglQ-mCh, GltI-YFP, and GltA-mCh in the presence of MglA^{Q82A}. All four fusion proteins generally also formed a single prominent cluster that retained a fixed position as cells moved (Fig. 4). Colocalization experiments showed

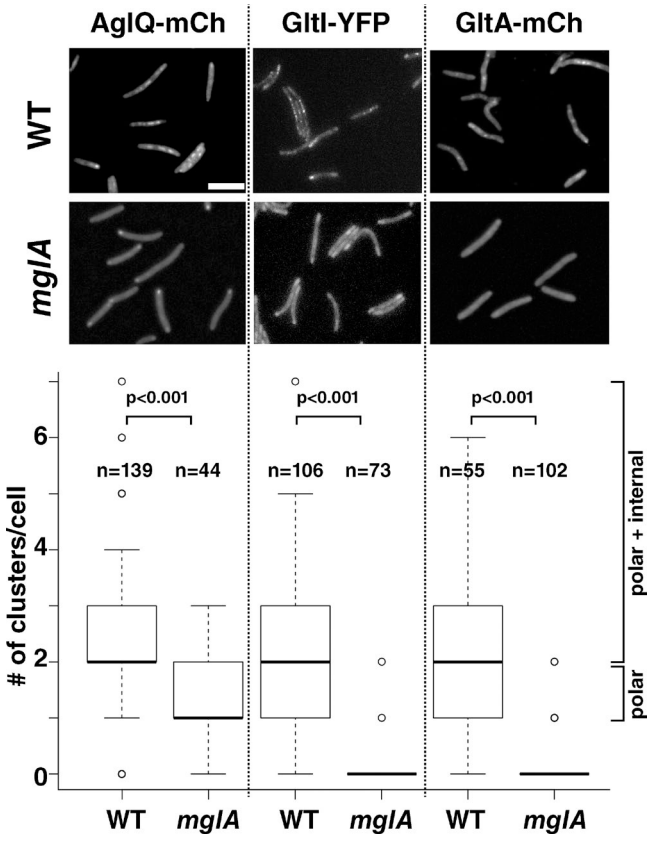

Figure 3. **MglA is required for assembly of the motility machinery.** Fluorescent clusters corresponding to GltI-YFP, AglQ-mCh, and GltA-mCh were detected and counted automatically as described in Materials and methods. The box plots represent cluster counts for each strain with the bottom and top boundaries of the boxes corresponding to the 25% and 75% percentiles, respectively. The median is shown as a thick black line and the whiskers represent the 10% and 90% percentiles. Outliers are shown as open circles. Note that in the *mglA* mutant, AglQ-mCh forms a polar cluster in many cells whereas GltI-YFP and GltA-mCh are diffusely localized. Therefore, in the absence of MglA the median of the AglQ-mCh cluster count is close to 1. *n* is the number of analyzed cells per strain. Statistics, *t test*. Bar, 4 µm.

that YFP-MglA^{Q82A} colocalized in the nonpolar cluster with AglZ-mCh and AglQ-mCh (Fig. 4, A–E). We conclude that in the presence of YFP-MglA^{Q82A} the Agl–Glt machinery mostly assembles to form a single prominent FA.

We next investigated which proteins of the motility machinery are important for the formation of the nonpolar cluster formed by YFP-MglA^{Q82A}. Because MglA is a cytosolic protein, its recruitment to the motility machinery would be expected to depend on a cytosolic protein or a cytosolic domain of a transmembrane protein of the machinery. We initially focused on GltI and AglZ, which are the only components of the motility machinery that are predicted to be entirely cytosolic. The nonpolar YFP-MglA^{Q82A} cluster was present in ∼50% of the total cell population in WT cells corresponding to the motile cells (Fig. 5, A and B). Consistent with the link between MglA and the Agl–Glt motility machinery, YFP-MglA^{Q82A} neither formed the prominent nonpolar cluster in the *aglZ* mutant nor in the *gltI* mutant while still forming clusters at both cell poles (Fig. 5, A and B). In contrast, YFP-MglA^{Q82A} still formed polar as well as nonpolar clusters in the *aglQ* mutant where the motility apparatus is assembled but paralyzed (Sun et al., 2011; Fig. 5, A and B). Importantly, in this mutant, the YFP-MglA^{Q82A} nonpolar clusters were also paralyzed. We conclude that formation of the nonpolar YFP-MglA^{Q82A} cluster depends on an intact Agl–Glt gliding machinery. Moreover, these data strongly support the notion that MglA is an integral part of the Agl–Glt gliding machinery. Because AglZ-YFP does not localize at FAs in a *gltI* mutant (Nan et al., 2010) and MglA interacts directly with AglZ (Yang et al., 2004; Mauriello et al., 2010), we favor a scenario in which MglA-GTP is incorporated into the Agl–Glt machinery by a direct interaction with AglZ, which is then connected to the rest of the machinery via GltI.

In total, we conclude that MglA associates with the cytoplasmic face of the Agl–Glt motility complex and because MglA^{Q82A} results in the formation of a single prominent Agl–Glt cluster, and MglA is required for the formation of AglQ-mCh, GltI-YFP, GltA-mCh, and AglZ-YFP clusters, MglA stimulates the assembly of the Agl–Glt complex at FAs.

The MreB cytoskeleton is required for the recruitment of MglA and the Agl–Glt machinery at FAs

MreB is required for the localization of AglZ to FAs and the two proteins interact directly (Mauriello et al., 2010). MreB is an essential protein in *M. xanthus* (Mauriello et al., 2010). Therefore, to test if MreB also functions in assembly of the entire Agl–Glt machinery, we interfered with MreB function by treating AglQ-mCh–expressing cells with A22, a compound that reduces MreB polymerization by binding to its nucleotide-binding pocket (Bean et al., 2009; van den Ent et al., 2014). These experiments were performed in a microfluidic chamber where the cells glide over glass treated with chitosan (Ducret et al., 2013). Injection of A22 in the chamber strongly reduced motility reversibly <1 min after addition (Fig. 6). Importantly, the nonpolar YFP-MglA^{Q82A} cluster but not the polar clusters was rapidly and reversibly dispersed by A22 (Fig. 6 A). Notably, AglQ-mCh clusters were also rapidly and reversibly dispersed by A22 treatment in otherwise WT cells (Fig. 6 B). In cells coexpressing YFP-MglA^{Q82A} and AglQ-mCh, A22 treatment also led to the simultaneous dispersal of the prominent nonpolar clusters formed by YFP-MglA^{Q82A} and AglQ-mCh (Fig. 6 C and Fig. S2). The effect of A22 on dispersal of motility complexes was specific because treatment with nigericin, a drug that dissipates the proton motive force and paralyzes the motility motor (Sun et al., 2011), stopped motility but did not disperse AglQ-mCh clusters; however, addition of A22 to nigericin-treated cells led to dispersal of the paralyzed motility complexes (Fig. 6 D). Moreover, the effects of A22 were specific for MreB because motility and YFP-MglA^{Q82A} localization in a strain containing the MreB^{V323A} variant, which binds A22 with a strongly reduced affinity (Bean et al., 2009), were unaffected by A22 (Fig. 6, E–G). We conclude that the MreB actin cytoskeleton is required for assembly of the MglA-containing Agl–Glt machinery at FAs.

MglA-GTP interacts with MreB polymers

AglZ interacts directly with MglA and MreB (Yang et al., 2004; Mauriello et al., 2010). To test if MreB and MglA also interact directly and if this interaction is nucleotide dependent, we first set up an in vitro interaction test. To this end, we took advantage of the recent discovery that an MreB variant that lacks the N-terminal amphipathic helix is soluble (His_6-$MreB_{\Delta Nt}$) and can be manipulated in vitro (Salje et al., 2011). The N-terminal amphi-

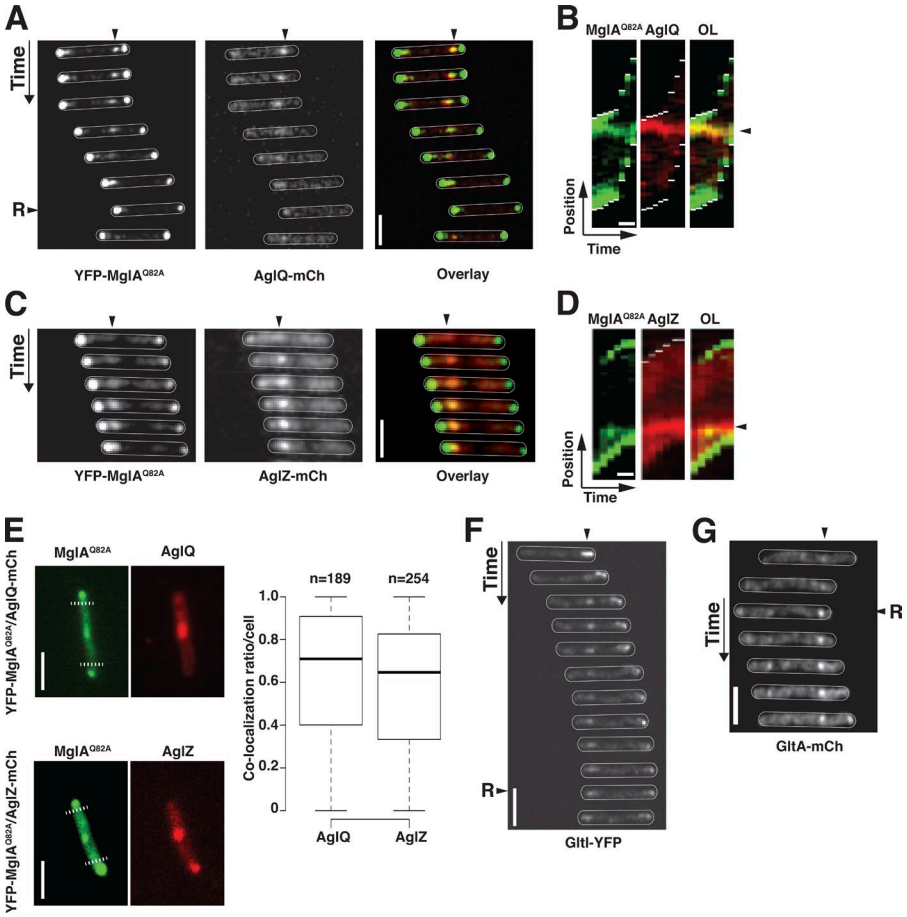

Figure 4. **MglA-GTP colocalizes with the AglGlt machinery.** (A and B) AglQ-mCh colocalizes with YFP-MglA^{Q82A}. (C and D) AglZ-mCh colocalizes with YFP-MglA^{Q82A}. 60-s time-lapse images and corresponding kymograph representations are shown. The cell outlines were obtained after overlaying with the phase-contrast images (not depicted). The black arrowheads indicate colocalizing clusters. R indicates a cellular reversal. (A) In the overlay, YFP-MglA^{Q82A} is shown in green and AglQ-mCh in red. (E) Colocalization analysis. For the AglZ-mCh/YFP-MglA^{Q82A} and the AglQ-mCh/YFP-MglA^{Q82A} pairs, the number of clusters that colocalize was determined by scoring YFP- and mCherry-bright nonpolar internal clusters. To only consider internal clusters, the poles were excluded for this analysis (dotted lines). (F and G) Localization of GltI-YFP and GltA-mCh in a strain expressing MglA^{Q82A}. Images were captured every 60 s. R indicates a cellular reversal. Bars: (A, B, and E–G) 2 µm; (C and D) 1 µm.

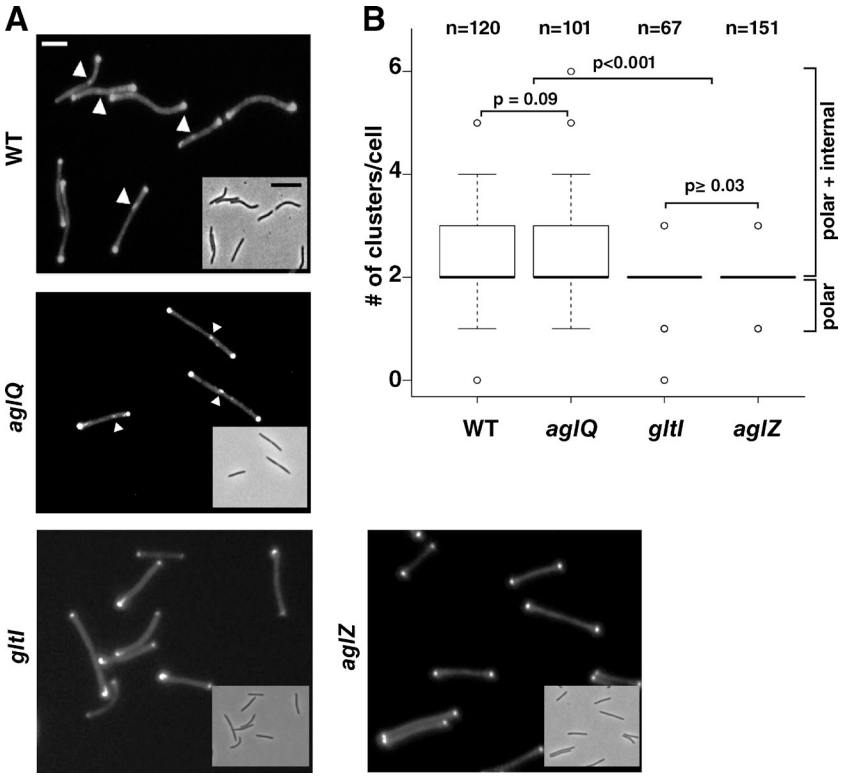

Figure 5. **Localization of YFP-MglA^{Q82A} to FA depends on cytoplasmic components of the motility complex.** (A) Localization of YFP-MglA^{Q82A} in mutants lacking a motor subunit (*aglQ*) or cytosolic components of the motility complex (*aglZ* and *gltI*). Arrowheads show FAs. Bar, 2 µm. Insets show corresponding phase-contrast images. Bar, 5 µm. (B) Box plot summary of YFP-MglA^{Q82A} localizations in the mutants shown in A. The boxplots read as in Fig. 3. Note that in the *gltI* and *aglZ* mutants, YFP-MglA^{Q82A} forms polar clusters in many cells. Therefore, in the absence of GltI or AglZ the median of the YFP-MglA^{Q82A} cluster count is close to 2. Statistics, *t test*.

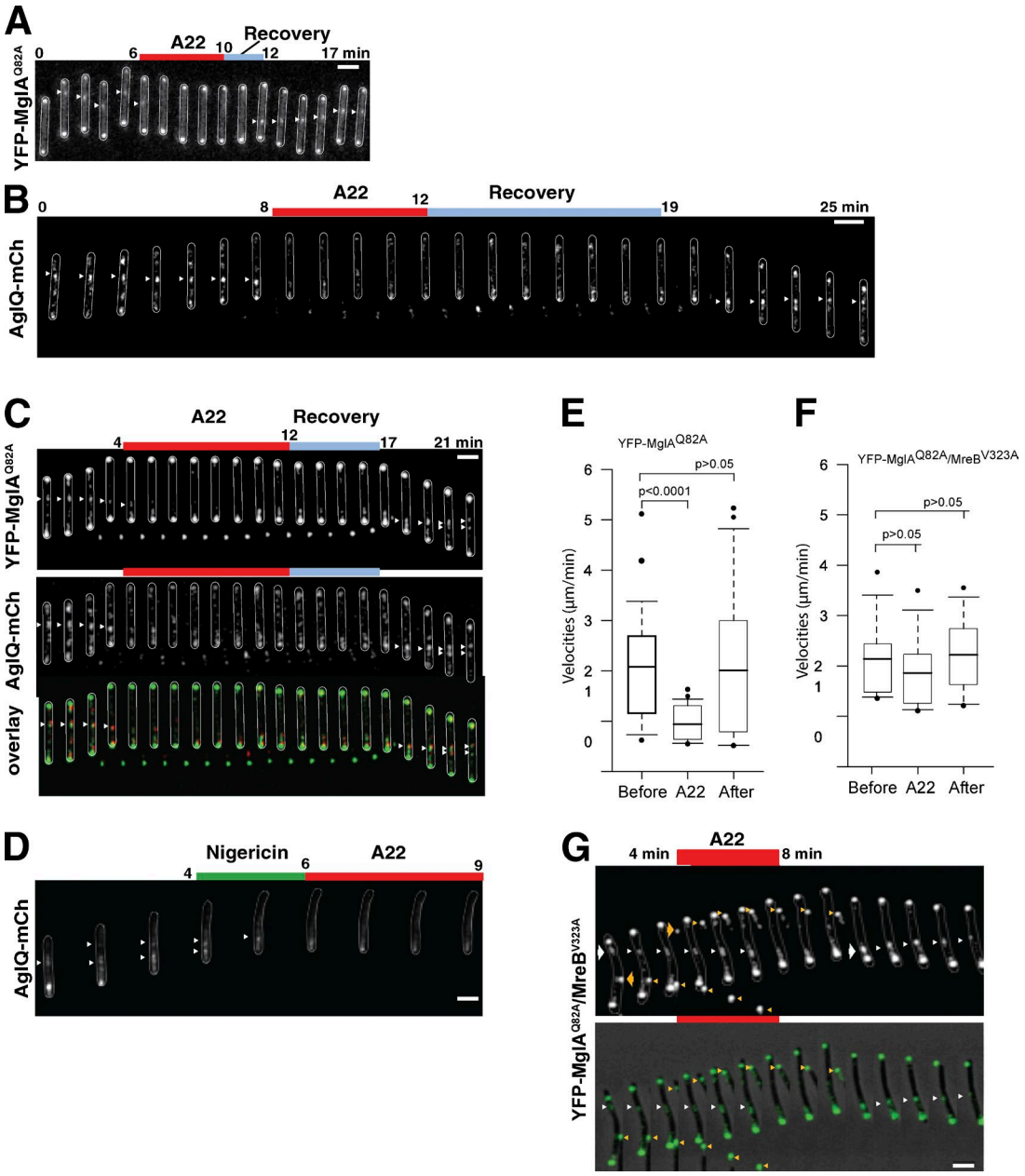

Figure 6. **MreB is important for motility and FA formation.** (A) A22 (10 µg/ml; red bar) disperses YFP-MglA^{Q82A} FA localization rapidly and reversibly. (A–C) Images were recorded every 60 s for 17 min. Note that motility stops immediately after A22 addition and resumes after a short recovery period (blue bar). Arrowheads indicate FAs. Bar, 1 µm. (B) A22 (10 µg/ml; red bar) disperses AglQ-mCh FA localization rapidly and reversibly in WT cells. Bar, 2 µm. (C) A22 (10 µg/ml; red bar) disperses colocalized YFP-MglA^{Q82A} and AglQ-mCh FAs rapidly and reversibly. In the overlay, the YFP-MglA^{Q82A} signal is indicated in green and the AglQ-mCh in red. Bar, 1 µm. (D) A22 disperses nigericin-paralyzed AglQ-mCh clusters in a WT background. Movement was first stopped by nigericin addition (100 µM; green bar) and A22 was further injected (10 µg/ml) 2 min after nigericin addition. Bar, 1 µm. (E and F) Box plots of the effect of A22 (10 µg/ml) on motility of cells expressing YFP-MglA^{Q82A} or YFP-MglA^{Q82A}/MreB^{V323A}. The box plots represent cluster counts for each strain with the bottom and top boundaries of the boxes corresponding to the 25% and 75% percentiles, respectively. The median is shown as a thick black line and the whiskers represent the 10% and 90% percentiles. Outliers are shown as closed circles. Statistics, *t test.* (G) A22 (10 µg/ml) does not perturb the formation of the YFP-MglA^{Q82A} cluster in cells expressing the MreB^{V323A} variant. Fluorescence images and a phase-contrast overlay are shown. White arrowheads indicate FA. Orange arrowheads indicate signals from neighboring cells that appear transiently in the field of view. Bar, 1 µm.

pathic helix is only important in vivo for an interaction between MreB and the bacterial membrane (Salje et al., 2011). *M. xanthus* His$_6$-MreB$_{\Delta Nt}$ could be purified as a soluble protein in a single step at high concentrations. The purified protein was functional and hydrolyzed ATP at rates that were similar to those described for the *Escherichia coli* and *Thermotoga maritima* MreB proteins (~0.04 min^{-1} at 300 mM KCl and ~0.07 min^{-1} at 75 mM KCl; Fig. 7 A and not depicted; Esue et al., 2005; Nurse and Marians, 2013). We next tested whether His$_6$-MreB$_{\Delta Nt}$ formed polymers in vitro by incubation at different temperatures in the presence of ATP. *M. xanthus* His$_6$-MreB$_{\Delta Nt}$ was recovered in the pellet fraction in a temperature- and time-dependent manner (Fig. 7 B and Fig. S3 A). To further analyze MreB polymerization, we performed dynamic light scattering (DLS) experiments in real time in the presence of ATP at various His$_6$-MreB$_{\Delta Nt}$ concentrations. Consistent with polymerization, a DLS signal was ob-

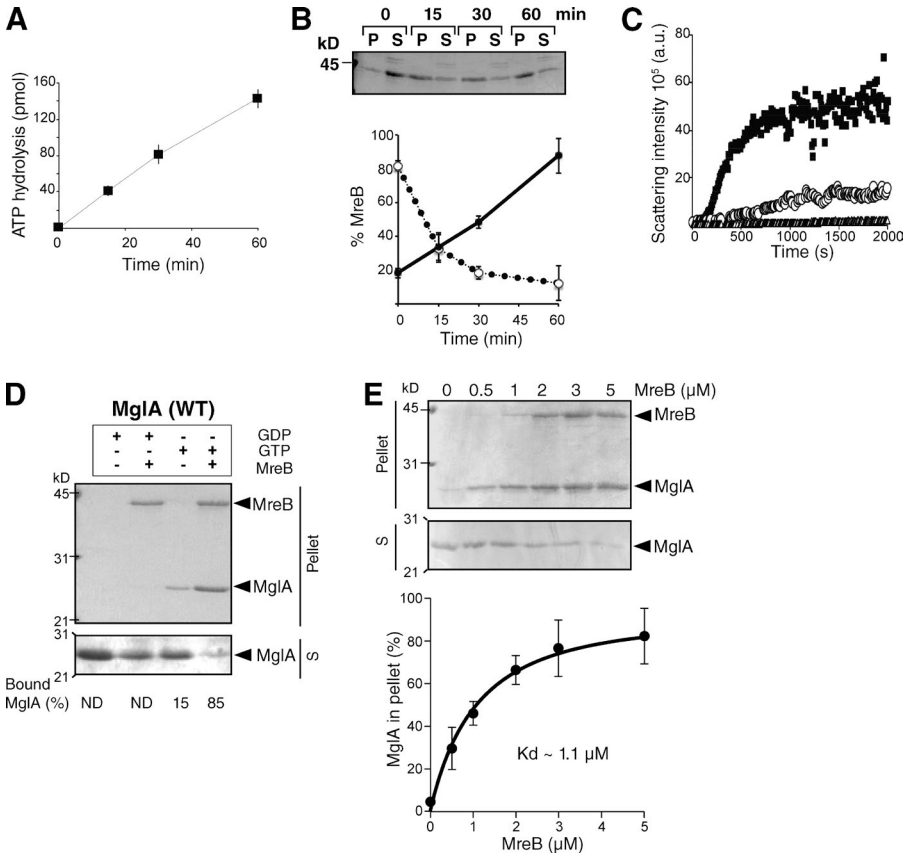

Figure 7. **MreB interacts directly with MglA-GTP.** (A) His_6-$MreB_{\Delta Nt}$ hydrolyzes ATP. His_6-$MreB_{\Delta Nt}$ (4 µM final concentration) was mixed with 50 µM ATPγ-[P^{32}] in 20 mM Tris, pH 7.4, 1 mM $MgCl_2$, and 300 mM KCl at 37°C. The results are mean values of triplicate measurements. (B) Kinetics of His_6-$MreB_{\Delta Nt}$ polymerization. Polymerization was induced by incubating His_6-$MreB_{\Delta Nt}$ (6.5 µM final concentration) in HKM buffer in the presence of 2 mM ATP at 37°C. A Coomassie-stained gel is shown. Relative protein amounts (arbitrary units) were measured over time in the pellets (black dots) and in the corresponding supernatants (open circles) in three independent experiments. (C) MreB forms polymers in a concentration-dependent manner. His_6-$MreB_{\Delta Nt}$ polymerization was measured by DLS. The scattering intensity was monitored immediately after addition of ATP (t = 0) at varying His_6-$MreB_{\Delta Nt}$ concentrations (8 µM [black squares], 4 µM [open circles], and 2 µM [open triangles]) in 20 mM Tris, pH 7.4, 1 mM $MgCl_2$, and 150 mM KCl at 37°C. (D) His_6-$MreB_{\Delta Nt}$ interacts directly with MglA-GTP. Polymerized His_6-$MreB_{\Delta Nt}$ (5 µM final concentration) in the presence of ATP was incubated with MglA-His_6 (2 µM final concentration) preloaded with GDP or GTP (1.0 mM) at 37°C, for 30 min, and interactions were tested in a sedimentation assay as described in A. Coomassie-stained gels of pellet and supernatant (S) fractions are shown. Bound MglA is expressed as the percentage of pellet-bound MglA over the total amount of MglA. ND, not detectable. (E) His_6-$MreB_{\Delta Nt}$ interacts with MglA-GTP in a concentration-dependent manner. The two proteins were mixed as in D and tested for interactions in the sedimentation assay. The MglA-binding curve was modeled with a bimolecular interaction scheme on the mean results of three independent experiments. The best fit was obtained for a K_d of ∼1.1 µM.

served in a concentration-dependent manner (Fig. 7 C). Further investigation of the polymerization properties indicated that it is nucleotide independent and extended filaments such as observed recently with *E. coli* MreB by electron microscopy were not observed (Fig. S3 B and not depicted; Nurse and Marians, 2013). The lack of dependence on nucleotide addition has also been observed for *Bacillus subtilis* and *Chlamydia pneumoniae* MreB (Mayer and Amann, 2009; Gaballah et al., 2011), and, in fact, imaging MreB filaments formed in vitro by electron microscopy has only been done successfully for *E. coli* MreB in mesophilic bacteria in the absence of added lipids (Nurse and Marians, 2013). The in vivo relevance of extended polymers is currently debated because MreB can form small patches or extended filaments depending on species and growth conditions (Domínguez-Escobar et al., 2011; Garner et al., 2011; Swulius et al., 2011; van Teeffelen et al., 2011; Reimold et al., 2013; van den Ent et al., 2014; Errington, 2015). Thus, in bacteria the length of MreB polymers may be subject to interactions with the membrane and other modes of regulation, complicating in vitro studies. Nevertheless, because cosedimentation assays have been used to detect specific MreB polymer–RodZ, MreB polymer–MurF, and MreB polymer–EF-Tu interactions in *E. coli*, *C. pneumoniae*, and *B. subtilis,* respectively (van den Ent et al., 2010; Gaballah et al., 2011; Defeu Soufo et al., 2015), we further proceeded to test interaction between MglA and MreB by cosedimentation.

We first tested the behavior of His_6-MglA-GDP and His_6-MglA-GTP during high-speed sedimentation in the absence of His_6-$MreB_{\Delta Nt}$. Under these conditions, MglA-GDP did not sediment in the presence of GDP and only a small fraction of MglA (15%) was recovered in the pellet in the presence of GTP (Fig. 7 D). In the presence of polymerized His_6-$MreB_{\Delta Nt}$, formed after incubation with ATP at 37°C for 30 min, MglA-GTP was significantly enriched in the pellet fraction (85% of the total amount of MglA; Fig. 7 D), whereas MglA-GDP was not and remained absent from the pellet fraction (Fig. 7 D). Similarly, an MglA-GTP–locked variant ($MglA^{Q82L}$), which has the same properties as $MglA^{Q82A}$ (Fig. S3 C; Zhang et al., 2010; Miertzschke et al., 2011), was enriched in the pellet fraction in the presence of GTP but not in the presence of GDP (Fig. S3 D). Importantly, MglA-GTP was recovered in the pellet in an MreB concentration–dependent manner, with an apparent K_d of 1.1 µM (Fig. 7 E). The interaction between MreB and MglA-GTP was highly specific because neither MglB nor BSA alone were copelleted with MreB polymers (Fig. S3 E).

MglB promotes disassembly of the motility complex at the lagging cell pole

Our findings that MglA-GTP is incorporated into the motility machinery and interacts with MreB could explain the puzzling observation that Agl–Glt motility complexes are disassembled

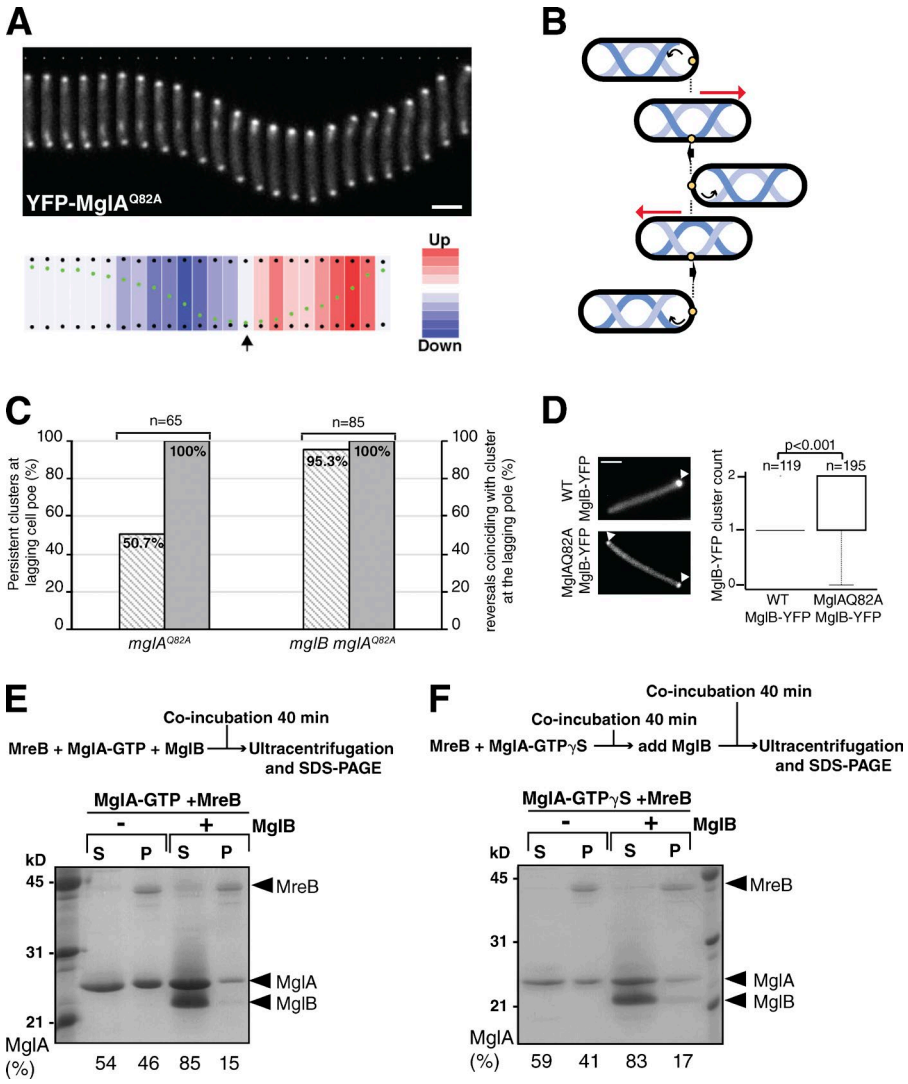

Figure 8. **MglB promotes disassembly of motility complexes at the lagging cell pole.** (A) Pendulum motion of cells expressing YFP-MglA^{Q82A}. Shown is a cell expressing YFP-MglA^{Q82A} and its associated motility diagram. Images were taken every 30 s. Movement is color coded in blue or red depending on direction, and higher color intensities reflect higher velocities. Note that the directional change (black arrow) occurs exactly when YFP-MglA^{Q82A} arrives at the lagging cell pole. Bar, 2 µm. (B) MglA^{Q82A}-dependent pendulum movement results from loss of spatial regulation of the motility machinery. In the presence of YFP-MglA^{Q82A} a single prominent FA is assembled. Because this FA is not disassembled at the lagging cell pole and may be attached to a helical track of unknown composition (Nan et al., 2011, 2013), movement is resumed in the opposite direction. (C) Inactivation of the motility complex at the lagging cell pole requires both MglB and its GAP activity. For any given strain, the percentage of persistent clusters at the lagging cell pole (striped bars) corresponds to the fraction of clusters arriving at the lagging cell pole that provoke a reversal. The correlation between reversals and clusters arriving at the lagging pole (gray bars) reflects the number of reversals that coincide with an arriving cluster. In the *mglA*^{Q82A} and *mglB mglA*^{Q82A} mutants, 100% of the reversals coincide with a cluster arriving at the lagging cell pole, but 50% of the clusters are dispersed in *mglA*^{Q82A} as opposed to the *mglB mglA*^{Q82A} where dispersal at the lagging pole is almost absent. (D) MglB-YFP is unipolar in WT cells and bipolar in MglA^{Q82A}-expressing cells. Polar fluorescent cluster counts (arrowheads) are shown for the WT and MglA^{Q82A} strains. Box plot reads as in Fig. 3. Statistics, *t test*. Bars, 2 µm. (E) MglB inhibits complex formation by His$_6$-MreB$_{\Delta Nt}$ and MglA-GTP. MglA-GTP (8 µM) was mixed with prepolymerized MreB (4 µM) in the presence or absence of MglB-His$_6$ (8 µM). Interaction with His$_6$-MreB$_{\Delta Nt}$ was tested in the sedimentation assay and revealed by Coomassie staining. (F) MglB dissociates MglA–MreB complexes. MglA-GTPγS–MreB complexes formed after 40-min coincubation were mixed or not with MglB-His$_6$ (8 µM) and further incubated for 40 min before ultracentrifugation. Interaction with His$_6$-MreB$_{\Delta Nt}$ was tested in the sedimentation assay and revealed by Coomassie staining.

at the lagging cell pole in WT cells: at this pole, interaction between MglA and MglB, the cognate MglA GAP, could cause the dissociation of MglA from MreB by stimulating GTP hydrolysis by MglA and/or by competing with MreB for MglA interaction, and thereby causing the disassembly of the motility complex. Consistent with such function and as opposed to WT cells that move several cell lengths before reversing their direction of movement, *mglB* mutant cells or cells expressing MglA^{Q82A} show a characteristic pendulum-like motion and reverse their direction of movement after moving a distance corresponding to one cell length (Zhang et al., 2010; Miertzschke et al., 2011). In YFP-MglA^{Q82A}–expressing cells, cellular reversals systematically appeared to coincide with a nonpolar cluster reaching the lagging cell pole (Fig. 8 A). These reversals likely arose from the constitutive activity of the gliding machinery because contrary to WT cells AglQ-mCh, GltA-mCh, and GltI-YFP clusters were not dispersed at the lagging cell pole in MglA^{Q82A}-expressing cells and in each case a reversal coincided with contact of the cluster with the lagging cell pole (Fig. 4, A, F, and G; and Fig. 8 B). Thus, in the absence of GTP hydrolysis on MglA, FAs are not repeatedly assembled and disassembled at the leading and lagging cell poles, respectively, giving rise to an oscillatory pendulum-like movement pattern as if the machinery was tracking endlessly along a closed helical loop path (Fig. 8 B; Nan et al., 2011). Similar pendulum motions have also been observed in *Plasmodium falciparum* TRAP mutants where FAs are improperly disengaged at the distal end of the parasite (Sibley, 2010).

Quantitative analysis showed that 100% of the reversal events in YFP-MglA^{Q82A}–expressing cells were correlated with a cluster reaching the lagging pole (Fig. 8 C). In contrast, only ∼50% of the clusters effectively provoked a reversal, suggesting

that nearly half of the clusters were still effectively dispersed at the lagging cell pole (Fig. 8 C). Thus another mechanism can partially compensate and induce the dispersal of MglA clusters in the absence of GTP hydrolysis, albeit at reduced efficiency (50%). Because MglB-YFP localizes to both cell poles in $MglA^{Q82A}$-expressing cells, contrary to WT cells where it localizes at one cell pole (Fig. 8 D), we reasoned that the presence of MglB might also compete with MreB for MglA interaction. Remarkably, YFP-$MglA^{Q82A}$ clusters were almost never dispersed at the lagging cell pole in the *mglB* mutant, despite the fact that YFP-$MglA^{Q82A}$ is not sensitive to the GAP activity of MglB (Fig. 8 C). In this strain, the arrival of a YFP-$MglA^{Q82A}$ cluster at the lagging pole systematically correlated with a reversal (Fig. 8 C). These observations suggest that MglB could additionally compete with MreB for MglA interaction, independently of its GAP activity.

We next tested if this competing effect could be observed in vitro. When equimolar amounts of MglA-GTP were coincubated with MglB and His_6-$MreB_{\Delta Nt}$, MglA-GTP was almost entirely recovered in the supernatant, as was MglB, and not in the pellet with His_6-$MreB_{\Delta Nt}$ (Fig. 8 E). This effect was not only a result of the activation of GTP hydrolysis by MglB because the same result was obtained when GTPγS, a nonhydrolysable form of GTP, was used (Fig. S3 F). Thus, MglB effectively competes with MreB for MglA interaction independently of its GAP activity. We next tested whether MglB addition can dissociate preformed MglA–MreB complexes. For this, we first allowed MglA–MreB complexes to form in the presence of GTPγS and subsequently added MglB. Again, we found that MglB was able to displace the MglA–MreB interaction (Fig. 8 F). We conclude that MglA-GTP interacts with MreB reversibly, allowing regulation by MglB. In vivo these interactions allow MglB to act in two complementary ways to unlatch the Agl–Glt complex from MreB at the lagging cell pole: (1) MglB activates MglA GTP hydrolysis by its GAP activity and (2) MglB physically competes for interaction with MreB.

The MreB motility function is independent from its role in PG synthesis

In rod-shaped bacteria, MreB is linked to the periplasmic PG synthesis machinery and forms patches that move in trajectories perpendicular to the cell axis powered by the PG synthesis machinery (Domínguez-Escobar et al., 2011; Garner et al., 2011; van Teeffelen et al., 2011). Blocking the PG synthesis machinery effectively blocks MreB motion. Of note, the effects of A22 on motility and protein localization in *M. xanthus* were quasi-instantaneous, observed at the minimum inhibitory concentration (MIC; 10 µg/ml; Fig. S4, A–C), several hours before any effects on cell morphology were evident (Fig. S4, A–C) and while PG synthesis was still ongoing (van Teeffelen et al., 2011). These observations suggest that the function of MreB in motility in *M. xanthus* is not linked to its function in PG synthesis. To test this possibility in a definitive manner, we treated *M. xanthus* cells with mecillinam, which blocks the transpeptidase activity of PBP2 and blocks MreB dynamics in *B. subtilis* and *E. coli* (Garner et al., 2011; van Teeffelen et al., 2011). Mecillinam neither had an effect on motility nor on the localization of YFP-$MglA^{Q82A}$ even when added at a concentration 15-fold higher than the MIC (10 µg/ml; Fig. 9, A and B; Fig. S5, A and B; and Table S3). Similarly, we tested a set of antibiotics that target different steps of PG synthesis and among which fosfomycin has also been shown to block MreB dynamics in *B. subtilis* and *E. coli* (Domínguez-Escobar et al., 2011; Garner et al., 2011; van Teeffelen et al., 2011). As a control, the translation inhibitor chloramphenicol was also included. Overall, with any given antibiotic, the treated cells were all motile, showing no or only minor motility defects at the MIC (Fig. 9 A and Table S3). As minor defects were also observed in the presence of chloramphenicol, we conclude that blocking PG synthesis does not block motility immediately, suggesting that the function of MreB in PG synthesis and therefore circumferential movements of MreB driven by the PG synthetic complex (Carballido-López et al., 2006; Garner et al., 2011; van Teeffelen et al., 2011) are independent of its function in motility and that the latter represent a coopted function.

Discussion

In total, the experiments reported here suggest a mechanism for the MglA-dependent spatial regulation of the motility complex (Fig. 10). The connection between the Agl–Glt complex and the MreB cytoskeleton is essential for its assembly and requires MglA because (a) the MreB inhibitor A22 disperses AglZ-YFP, YFP-$MglA^{Q82A}$, and AglQ-mCh clusters (Mauriello et al., 2010; this study), (b) AglZ-YFP, AglQ-mCh, GltA-mCh, and GltI-YFP clusters are not observed in the absence of MglA (Mauriello et al., 2010; this study), and (c) MreB interacts with MglA-GTP specifically, i.e., MreB did not interact with MglA-GDP, MglB, or BSA. Importantly, addition of MglB competed with MreB for MglA interaction and even when MglA–MreB complexes had been preformed, showing that the MglA–MreB interaction is reversible and sensitive to the presence of MglB. In total, these results suggest that a protein interaction network involving all pairwise interactions between MreB, MglA-GTP, and AglZ connect the motility machinery with the MreB cytoskeleton at the leading cell pole (Fig. 10). The exact interactions with the motility machinery still need to be defined and may require GltI and, as recently proposed by Nan et al. (2015), AglR, a component of the Agl motor. After interaction with MreB, the Agl–Glt machinery together with MglA-GTP and MreB would become active and move directionally along its elusive track toward the lagging cell pole. It is unlikely that MreB itself forms the track because MreB does not appear to make continuous and polarized filaments in bacterial cells (Domínguez-Escobar et al., 2011; Garner et al., 2011; van Teeffelen et al., 2011) but instead MreB could act as a protein scaffold for assembly of the motility machinery. Recently, Nan et al. (2015) further suggested that MglA also regulates the directionality of the Agl motor; whether this is linked to the interaction with MreB remains to be explored. The incorporation of MglA-GTP into the motility machinery makes the stability of motility complexes sensitive to both the presence of MglA and its nucleotide-bound state. This provides a simple mechanism for the disassembly of the motility complex at the lagging cell pole: the action of MglB results in the dissociation from MreB by two complementary mechanisms, spatial activation of MglA-GTP hydrolysis and direct competition for interaction with MreB (Fig. 10). This spatial control is essential to allow persistent movements and thus to prevent the system from reversing its direction of movement and generate futile pendulum movements. Of note, pendulum motions must not be confused

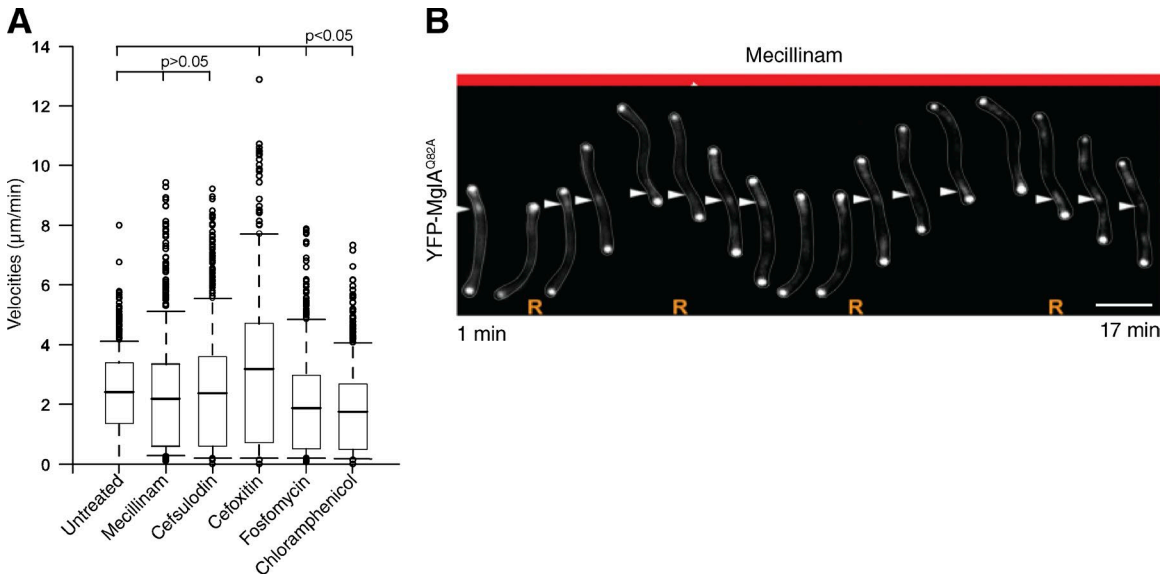

Figure 9. **High concentrations of mecillinam and other PG synthesis–blocking antibiotics do not block motility on short time scales.** (A) Effect of PG synthesis–blocking antibiotics on motility at the MIC. Velocities were calculated from time-lapse recordings in which cells were recorded at 30-s intervals for 10 min. The box plots read as in Fig. 3. (B) Pendulum motion and YFP-MglA^{Q82A} cluster formation is still observed in the presence of 150 µg/ml mecillinam. The MIC of mecillinam is 10 µg/ml. Arrowheads point to fixed YFP-MglA82A clusters. Bar, 2 µm.

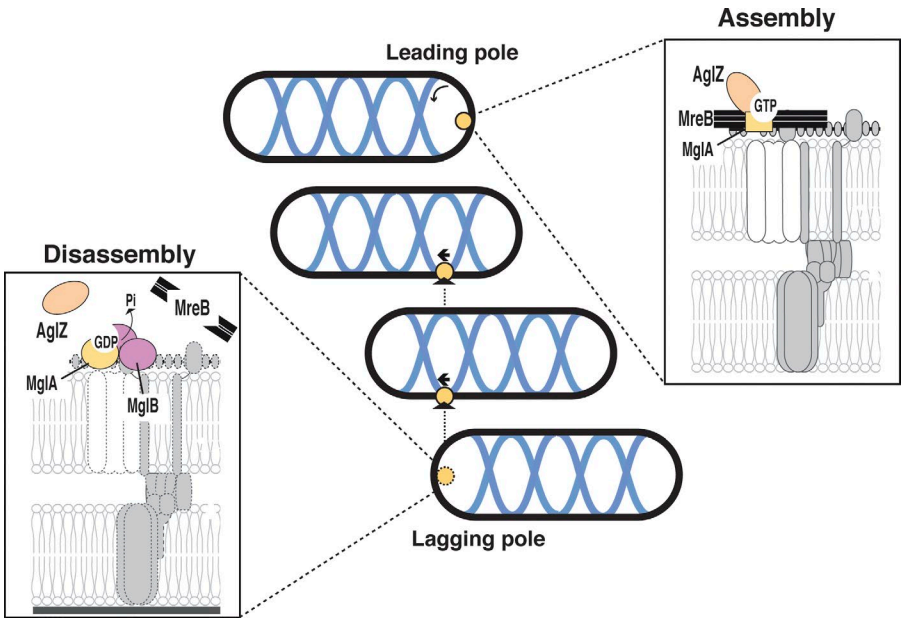

Figure 10. **Spatial regulation of the motility complexes in *M. xanthus*.** Spatial control of the gliding motility complex is proposed to be controlled by an interaction network involving at least four proteins, MglA, MreB, AglZ, and MglB. At the leading cell pole, MglA-GTP (orange square) interacts with AglZ and MreB, which creates a scaffold for the motility complex via downstream interactions to AglZ and possibly other proteins of the motility complex, e.g., AglR, a component of the molecular motor (Nan et al., 2015). The exact assembly pathway remains to be determined. For clarity, a single motility complex is shown, but several motility complexes can be assembled in the same cell as shown in Fig. 1. When the motility complex reaches the lagging cell pole (dotted circle), it encounters MglB, which acts in two complementary ways to dissociate MglA from the MreB cytoskeleton: (1) it promotes the conversion to MglA-GDP (orange circle) and (2) it physically competes with MreB breaking the interaction between MglA and MreB. The removal of MglA from the motility complexes promotes its disassembly (pictured by dashed lines). Although disassembly of the entire complex is suggested, the exact disassembly pathway is not known and some subcomplexes could persist and be recruited again at the new leading cell pole for a new motility cycle.

with regulated reversals, a process whereby *M. xanthus* cells change their direction of movement by switching the localization of MglA and MglB simultaneously (Leonardy et al., 2010; Zhang et al., 2010). Regulated reversals are essential for *M. xanthus* multicellular behaviors and, in this case, the reversal switch is activated by the signaling activity of the Frz chemosensory system, a bacterial chemosensory that responds to environmental signals (Keilberg and Søgaard-Andersen, 2014). Thus, MglA has a dual function and it is both a spatial regulator of assembly and an intrinsic component of the motility machinery. Remarkably, in eukaryotic cells small Ras-like G-proteins also act downstream from signal transduction pathways (i.e., G-protein–coupled receptors) to regulate the front–rear assembly/disassembly of the actin cytoskeleton and FA formation during motility (Raftopoulou and Hall, 2004; Charest and Firtel, 2007). Thus, the *M. xanthus* motility system represents a fascinating example of convergent evolution in the regulation of assembly/disassembly processes involved in motility.

Although the bacterial MreB cytoskeleton was discovered more than a decade ago, only a few direct-binding partners have been identified, most of them coupling MreB to the PG syn-

thesis machinery (Typas et al., 2012). We show that MreB is involved in bacterial motility through a direct and specific interaction with MglA-GTP, the active form of MglA, and AglZ as reported previously (Mauriello et al., 2010) to stimulate the assembly of Agl–Glt motility complexes at FAs. Two lines of evidence suggest that this function is independent of the function of MreB in PG synthesis: (1) antibiotics that immediately block PG synthesis and block MreB dynamics do not block motility; and (2) A22 that targets MreB directly but does not block PG synthesis immediately, blocks motility instantaneously. In *M. xanthus*, the MreB actin-like cytoskeleton also functions as a scaffold for the PG synthesis machinery, as shown by long-term effects of A22 (Fig. S4) but it may also have been coopted by the gliding motility machinery and function independently as a scaffold for formation of the Agl–Glt machinery. Thus, studying the connection between the Agl–Glt complex and MreB may more generally reveal new accessory functions of the bacterial cytoskeleton.

Materials and methods

Bacterial strains, plasmids, and growth

DK1622 was used as the WT *M. xanthus* strain throughout and all *M. xanthus* strains used are derivatives of DK1622. *M. xanthus* strains used are listed in Table S1. Plasmids are listed in Table S2. All plasmids were verified by sequencing. *M. xanthus* strains were grown at 32°C in 1% CTT broth (Hodgkin and Kaiser, 1977) and on CTT agar plates supplemented with 1.5% agar. Kanamycin (50 µg/ml) or oxytetracycline (10 µg/ml) was added when appropriate. In-frame deletions were generated by overlap PCR containing ∼750 bp upstream and downstream of the desired mutant region and cloned in pBJ114 or pBJ113 plasmids. The plasmids were transformed by electroporation into the appropriate strain and the integration via homologous recombination (or by site-specific recombination at the Mx8 *attB* site for fluorescent fusions) was selected by antibiotic resistance. For in-frame deletions the transformants were further grown on galactose to excise the plasmid via a second homologous recombination. All strains generated were verified by PCR.

Determination of MIC

To determine MIC, exponentially growing cells of DK1622 were diluted into prewarmed CTT growth medium containing different concentrations of the relevant drugs. Cell growth and cell shape was analyzed for at least 24 h after addition of a drug by measuring OD_{550} and by phase-contrast microscopy every 3 h. The following drugs were tested: A22 (EMD Millipore), mecillinam, cefoxitin, fosfomycin, cefsulodin, and chloramphenicol (Sigma-Aldrich).

Drug injection experiments in flow chamber

For A22 injection experiments, *M. xanthus* cells were immobilized on a chitosan-coated surface, as described previously (Ducret et al., 2013). In brief, custom-built polydimethylsiloxane microfluidic glass chambers were coated with chitosan solution and washed after 30 min. Chambers were further rinsed with 1 ml TPMG buffer (10 mM Tris-HCl, pH 7.6, 8 mM $MgSO_4$, 1 mM KH_2PO_4, and 100 mM glucose). Subsequently, 1 ml of an exponentially growing culture was injected into the chamber and left for 30 min without flow. Unattached cells were removed by rinsing with 1 ml TPMG by manual injection and time-lapse microscopy on attached cells was performed. A22 was injected manually at a final concentration of 10 µg/ml a few minutes after cells were confirmed to be motile. Immediately upon detection of an effect on motility, 1–2 ml TPMG buffer was injected to test for reversibility.

Fluorescence microscopy

For phase-contrast and fluorescence microscopy, cells from exponentially growing cultures were transferred to a thin 1% agar pad with TPM buffer (10 mM Tris-HCl, pH 7.6, 8 mM $MgSO_4$, and 1 mM KH_2PO_4) on a glass slide and covered with a coverslip. After 15 min, GFP or m-cherry fluorochromes were visualized at 32°C using either a temperature-controlled DM6000B microscope (Leica) with a Plan Apochromat 100×/NA 1.40 oil objective (Leica) and a Cascade II 1024 camera (Roper Scientific) or a temperature-controlled TE2000-E-PFS microscope (Nikon) with a 100×/1.4 DLL objective and a CoolSNAP HQ2 camera (Photometrics). Images were recorded and processed with Metamorph software (Molecular Devices).

Motility assays and drug experiments on agar

M. xanthus cells from an exponentially grown culture in CTT were mixed with the relevant drug at various concentrations. Subsequently, 10 µl of the cell suspension was transferred to a microscope slide covered with a thin 1% agarose pad buffered with TPM buffer and supplemented with the same concentration of the relevant drug. Cells were immediately covered with a coverslip and motility and protein localization immediately followed for 10–15 min at 32°C. Time-lapse microscopy was done using a DMI6000B microscope (Leica) with a Plan Apochromat 100×/NA 1.40 phase-contrast oil objective (Leica) using appropriate filters and with images captured using a Flash 4.0 camera (Hamamatsu Photonics). Images were processed as described in the Cell tracking and image analysis section.

Cell tracking and image analysis

The image analysis was performed with FIJI/ImageJ free software. To perform the routine analysis on microscopy images and time-lapse (cell tracking, FA detection, kymograph, cluster detection, etc.), we developed our own collection of plugins. Plugin codes are available in the online supplemental material. Each plugin was coded in Python. In brief, the phase-contrast image of rod-shaped cells provides the mask of cell bodies and yields morphological parameters especially the longitudinal axis. This allows a straighten operation and the axis is used as a reference frame for the cluster localization. Because the internal clusters are of weak intensity, the images were denoised by applying a neutral density filter and background subtraction. The presence of fluorescent clusters was systematically verified on the unprocessed images to ascertain that the procedures did not generate artifact signals. For dynamic tracking a simple algorithm of nearest objects was used. For each cell identified at frame t, a circular region with a radius equal to the maximum displacement step was exanimated in frame t + 1; the nearest cell in this region was linked to the same track. Results were validated manually. Velocities were calculated from the tracking results (Δdisplacement/Δtime). The points of the trajectory (x0, x1, … , xn; y0, y1, … , yn) were used to calculate the mean square displacement (MSD) at time $t = d^2_t = (x_t - x_{t-1})^2 + (y_t - y_{t-1})^2$:

$$\mathrm{MSD}(t) = \frac{1}{t}\sum_{0}^{t} d_t^2$$

This was calculated with an R software script.

Colocalization ratios were calculated by generating a mask of the fluorescent areas occupied by each fluorescent protein and reporting the colocalized area to the total area of AglZ-mCh or AglQ-mCh: (YFP-MglA∩AglZ-mCh)/AglZ-mCh; (YFP-MglA∩AglQ-mCh)/AglQ-mCh.

Data analysis, figure charts, and statistics were performed with the R software.

Protein expression and purification

MglA-His_6 proteins, MglB-His_6, and His_6-$MreB_{\Delta Nt}$ were purified essentially as previously described (Mauriello et al., 2010; Zhang et al., 2010). In brief, overexpression of the MglA-His_6, MglB-His_6, and His_6-$MreB_{\Delta Nt}$ proteins was induced by growing C41 (DE3; F – *ompT hsdSB [rB– mB–] gal dcm* [λDE3]) containing the relevant plasmids at 20°C for 20 h in the presence of 0.5 mM IPTG. The same procedure was used to purify MglA-His_6 and MglB-His_6 except that GDP was not added at the final steps of the MglB purification. Cells containing MglA-His_6 or MglB-His_6 were harvested by centrifugation at 10,000 *g* for 10 min; resuspended in a buffer containing 50 mM NaH_2PO_4, pH 8.0, 300 mM NaCl, 10 mM imidazole, and 10% glycerol (vol/vol); and lysed using a French press. Cells overexpressing MreB-His_6 were lysed in 20 mM Tris-HCl, pH 7.4, 300 mM NaCl, 1 mM $MgCl_2$, 0.1% (wt/vol) CHAPS, 30 mM imidazole supplemented with a protease inhibitor cocktail (Roche), and 0.25 mM PMSF using a French press. Lysates were centrifuged twice (20,000 *g* at 4°C for 30 min) to remove debris. For MglA/MglB, supernatants were incubated with Nickel beads (Bio-Rad Laboratories) for 1 h at 4°C, and then beads were collected and loaded onto a 5-ml HisTrap column (GE Healthcare). The elution was performed using a buffer containing 50 mM NaH_2PO_4, pH 8.0, 300 mM NaCl, and 250 mM imidazole, and for MglA, GDP 30 µM. To purify His_6-$MreB_{\Delta Nt}$, the supernatant obtained after the clearing centrifugation was incubated with Nickel beads for 2 h at 4°C. Subsequently, the beads were collected and loaded onto a 5-ml HisTrap column. Protein was eluted using a buffer containing 20 mM Tris-HCl, pH 7.4, 300 mM NaCl, 1 mM $MgCl_2$, 0.1% (wt/vol) CHAPS, 250 mM imidazole, 0.25 mM PMSF, and 10% glycerol (vol/vol). Protein purification was analyzed using SDS-PAGE, and protein concentrations were quantified using Bradford assay (Bio-Rad Laboratories).

Polymerization and high speed sedimentation of His_6-$MreB_{\Delta Nt}$

To analyze filament formation by His_6-$MreB_{\Delta Nt}$, the protein was precentrifuged at 100,000 *g* for 15 min at 4°C. His_6-$MreB_{\Delta Nt}$ at the indicated concentrations was incubated in HKM buffer (40 mM Hepes, pH 7.7, 300 mM KCl, 2 mM $MgCl_2$, and 1 mM DTT) and 2 mM nucleotide (ATP, ADP, GDP, or GTP as indicated). Samples were incubated at 4°C, 25°C, or 37°C for 10, 15, 30, or 60 min. Subsequently, samples were used for high-speed sedimentation. For high-speed sedimentation, samples were centrifuged at 70,000 *g* for 15 min at 4°C. The separated supernatant and pellet were dissolved in SDS loading buffer and analyzed by SDS-PAGE. Equivalent volumes of the supernatant and pellet were loaded on the gel and stained with Coomassie blue G250.

ATPase assay

ATPase activity was measured using a radioactive charcoal-based assay (Rasmussen et al., 1998). In brief, His_6-$MreB_{\Delta Nt}$ at 4 µM was incubated in 20 mM Tris, pH 7.4, 1 mM $MgCl_2$, 50 µM ATPγ-[P^{32}] (500 dpm/pmol), and 300 mM KCl (unless otherwise stated) at 37°C for the indicated times. ATP hydrolysis was terminated by transferring 20-µl aliquots of the reaction into a 500-µl slurry containing acid-washed charcoal. The charcoal was removed by centrifugation (5 min at 16,000 *g*) and the amount of radioactivity present in the supernatant was determined by liquid scintillation counting.

DLS

All measurements were made using a Dynapro MSX instrument (Protein Solutions) equipped with a Peltier temperature controller. A 15-µl solution containing His_6-$MreB_{\Delta Nt}$ (concentration from 2 to 8 µM as indicated in the figure legends) was obtained by dilution in 20 mM Tris, pH 7.4, 1 mM $MgCl_2$, 150 mM KCl, and 1 mM ATP. After equilibration at 37°C in a quartz cuvette, 10 autocorrelation functions of the scattered light were determined at the optimal laser intensity, each for 10 s.

In vitro interaction between MglA-His_6 proteins and His_6-$MreB_{\Delta Nt}$

Purified MglA-His_6 and $MglA^{Q82L}$-His_6 (10 µM final concentration) were first loaded with GDP or GTP in a buffer containing 160 mM Hepes, 300 mM KCl, 2 mM $MgCl_2$, and 1 mM GDP or GTP for 30 min at 25°C. MreB-His_6 (6.5 µM final concentration) was polymerized for 60 min at 37°C as described. Subsequently, His_6-$MreB_{\Delta Nt}$ was mixed with GDP- or GTP-loaded MglA-His_6 giving a final concentration of His_6-$MreB_{\Delta Nt}$ of 5 µM and of MglA-His_6 proteins of 2 µM. Samples were incubated for 30 min at 25°C and high speed sedimentation done as described. The addition of MglA-His_6 did not significantly change the polymerization kinetics of MreB-His_6. To analyze the concentration-dependent effect of polymerized MreB-His_6 on sedimentation of MglA-His_6, His_6-$MreB_{\Delta Nt}$ was polymerized as described and MglA-His_6 was GTP loaded as described. After mixing, the concentration of MglA-His_6 was held constant at 2 µM and the concentration of MreB-His_6 varied from 0 to 5 µM.

Competition between MreB and MglB for binding to MglA

Purified MglA-His_6 was first loaded with GTP in HKM buffer supplemented with 1 mM GTP for 60 min at 25°C. His_6-$MreB_{\Delta Nt}$ (4 µM final concentration) was polymerized for 60 min at 37°C as described. Subsequently, His_6-$MreB_{\Delta Nt}$ was mixed with GTP-loaded MglA-His_6 (8 µM) and with or without MglB-His_6 (8 µM). Samples were incubated for 40 min at 25°C and high speed centrifuged at 70,000 *g* for 15 min at 4°C. For competition of preformed MglA-GTP–MreB complexes, the MglA–MreB complexes were first allowed to form as described in the previous paragraph and MglB was added, again at equimolar concentrations.

Online supplemental material

Fig. S1 provides supporting data on the membrane localization of GltA-mCh and cytosolic localization of GltI-YFP and provides single motility analyzes of the WT, *aglQ*, *gltI*, and *aglZ* mutants. Fig. S2 shows the effect of A22 on AglQ-mCh and YFP-$MglA^{Q82A}$ on a kymograph representation. Fig. S3 provides supporting information that MreB polymers interact with MglA-GTP. Fig. S4 shows the effect of A22 on growth and cell shape. Fig. S5 shows the effect of mecillinam on growth and cell shape. Tables S1 and S2 list the strains and plasmids used in this study. Table S3 lists the MIC of various antibiotics used in this study. All source codes are written in Python for their use as FIJI plugins. The package includes bacterial cell morphometric analysis, tracking, and graphic representation plugins. Online supplemental material is available at http://www.jcb.org/cgi/content/full/jcb.201412047/DC1.

Acknowledgments

Dr. Alan Hall served as an editor of this manuscript in its early stages and he provided critical, constructive, and encouraging comments that were invaluable to us. We dedicate this manuscript in his memory.

We thank Nassos Typas for helpful discussions. We thank Emilia Mauriello and Frédéric Luton for comments on the manuscript. We thank Steffi Lindow for excellent technical assistance and Carole Baron-Gaillard for advice and for MglA and MglB purification. We thank Benedikt von der Heyde for constructing strain SA6508.

L. Søgaard-Andersen is supported by the German Research Council within the framework of the Graduate School "Intra- and Intercellular Transport and Communication," the Landes-Offensive zur Entwicklung wissenschaftlich-ökonomischer Exzellenz Research Center for Synthetic Microbiology, and the Max Planck Society. M. Franco is supported by a European Research Council starting grant (DOME-261105

to T. Mignot) and the French National Research Agency through the Investments for the Future Labex SIGNALIFE (program reference #ANR-11-LABX-0028-01). T. Mignot is supported by a Prix coup d'élan pour la Recherche Française 2011 of the Bettencourt-Schueller Foundation and a European Research Center starting grant (DOME-261105).

The authors declare no competing financial interests.

Submitted: 9 December 2014
Accepted: 9 June 2015

References

Balagam, R., D.B. Litwin, F. Czerwinski, M. Sun, H.B. Kaplan, J.W. Shaevitz, and O.A. Igoshin. 2014. *Myxococcus xanthus* gliding motors are elastically coupled to the substrate as predicted by the focal adhesion model of gliding motility. *PLOS Comput. Biol.* 10:e1003619. http://dx.doi.org/10.1371/journal.pcbi.1003619

Bean, G.J., S.T. Flickinger, W.M. Westler, M.E. McCully, D. Sept, D.B. Weibel, and K.J. Amann. 2009. A22 disrupts the bacterial actin cytoskeleton by directly binding and inducing a low-affinity state in MreB. *Biochemistry.* 48:4852–4857. http://dx.doi.org/10.1021/bi900014d

Carballido-López, R., A. Formstone, Y. Li, S.D. Ehrlich, P. Noirot, and J. Errington. 2006. Actin homolog MreBH governs cell morphogenesis by localization of the cell wall hydrolase LytE. *Dev. Cell.* 11:399–409. http://dx.doi.org/10.1016/j.devcel.2006.07.017

Charest, P.G., and R.A. Firtel. 2007. Big roles for small GTPases in the control of directed cell movement. *Biochem. J.* 401:377–390. http://dx.doi.org/10.1042/BJ20061432

Defeu Soufo, H.J., C. Reimold, H. Breddermann, H.G. Mannherz, and P.L. Graumann. 2015. Translation elongation factor EF-Tu modulates filament formation of actin-like MreB protein in vitro. *J. Mol. Biol.* 427:1715–1727. http://dx.doi.org/10.1016/j.jmb.2015.01.025

Domínguez-Escobar, J., A. Chastanet, A.H. Crevenna, V. Fromion, R. Wedlich-Söldner, and R. Carballido-López. 2011. Processive movement of MreB-associated cell wall biosynthetic complexes in bacteria. *Science.* 333:225–228. http://dx.doi.org/10.1126/science.1203466

Ducret, A., O. Théodoly, and T. Mignot. 2013. Single cell microfluidic studies of bacterial motility. *Methods Mol. Biol.* 966:97–107.

Errington, J. 2015. Bacterial morphogenesis and the enigmatic MreB helix. *Nat. Rev. Microbiol.* 13:241–248. http://dx.doi.org/10.1038/nrmicro3398

Esue, O., M. Cordero, D. Wirtz, and Y. Tseng. 2005. The assembly of MreB, a prokaryotic homolog of actin. *J. Biol. Chem.* 280:2628–2635. http://dx.doi.org/10.1074/jbc.M410298200

Gaballah, A., A. Kloeckner, C. Otten, H.-G. Sahl, and B. Henrichfreise. 2011. Functional analysis of the cytoskeleton protein MreB from *Chlamydophila pneumoniae*. *PLoS ONE.* 6:e25129. http://dx.doi.org/10.1371/journal.pone.0025129

Garner, E.C., R. Bernard, W. Wang, X. Zhuang, D.Z. Rudner, and T. Mitchison. 2011. Coupled, circumferential motions of the cell wall synthesis machinery and MreB filaments in *B. subtilis*. *Science.* 333:222–225. http://dx.doi.org/10.1126/science.1203285

Harshey, R.M. 2003. Bacterial motility on a surface: many ways to a common goal. *Annu. Rev. Microbiol.* 57:249–273. http://dx.doi.org/10.1146/annurev.micro.57.030502.091014

Heasman, S.J., and A.J. Ridley. 2008. Mammalian Rho GTPases: new insights into their functions from in vivo studies. *Nat. Rev. Mol. Cell Biol.* 9:690–701. http://dx.doi.org/10.1038/nrm2476

Hodgkin, J., and D. Kaiser. 1977. Cell-to-cell stimulation of movement in nonmotile mutants of *Myxococcus*. *Proc. Natl. Acad. Sci. USA.* 74:2938–2942. http://dx.doi.org/10.1073/pnas.74.7.2938

Hodgkin, J., and D. Kaiser. 1979. Genetics of gliding motility in *Myxococcus xanthus* (Myxobacterales): Genes controlling movement of single cells. *Mol. Gen. Genet.* 171:167–176. http://dx.doi.org/10.1007/BF00270003

Holkenbrink, C., E. Hoiczyk, J. Kahnt, and P.I. Higgs. 2014. Synthesis and assembly of a novel glycan layer in *Myxococcus xanthus* spores. *J. Biol. Chem.* 289:32364–32378. http://dx.doi.org/10.1074/jbc.M114.595504

Jakobczak, B., D. Keilberg, K. Wuichet, and L. Søgaard-Andersen. 2015. Contact- and protein transfer–dependent stimulation of assembly of the gliding motility machinery in *Myxococcus xanthus. PLoS Genet.* In Press.

Jarrell, K.F., and M.J. McBride. 2008. The surprisingly diverse ways that prokaryotes move. *Nat. Rev. Microbiol.* 6:466–476. http://dx.doi.org/10.1038/nrmicro1900

Keilberg, D., and L. Søgaard-Andersen. 2014. Regulation of bacterial cell polarity by small GTPases. *Biochemistry.* 53:1899–1907. http://dx.doi.org/10.1021/bi500141f

Keilberg, D., K. Wuichet, F. Drescher, and L. Søgaard-Andersen. 2012. A response regulator interfaces between the Frz chemosensory system and the MglA/MglB GTPase/GAP module to regulate polarity in *Myxococcus xanthus*. *PLoS Genet.* 8:e1002951. http://dx.doi.org/10.1371/journal.pgen.1002951

Leonardy, S., M. Miertzschke, I. Bulyha, E. Sperling, A. Wittinghofer, and L. Søgaard-Andersen. 2010. Regulation of dynamic polarity switching in bacteria by a Ras-like G-protein and its cognate GAP. *EMBO J.* 29:2276–2289. http://dx.doi.org/10.1038/emboj.2010.114

Luciano, J., R. Agrebi, A.V. Le Gall, M. Wartel, F. Fiegna, A. Ducret, C. Brochier-Armanet, and T. Mignot. 2011. Emergence and modular evolution of a novel motility machinery in bacteria. *PLoS Genet.* 7:e1002268. http://dx.doi.org/10.1371/journal.pgen.1002268

Mauriello, E.M., B. Nan, and D.R. Zusman. 2009. AglZ regulates adventurous (A-) motility in *Myxococcus xanthus* through its interaction with the cytoplasmic receptor, FrzCD. *Mol. Microbiol.* 72:964–977. http://dx.doi.org/10.1111/j.1365-2958.2009.06697.x

Mauriello, E.M.F., F. Mouhamar, B. Nan, A. Ducret, D. Dai, D.R. Zusman, and T. Mignot. 2010. Bacterial motility complexes require the actin-like protein, MreB and the Ras homologue, MglA. *EMBO J.* 29:315–326. http://dx.doi.org/10.1038/emboj.2009.356

Mayer, J.A., and K.J. Amann. 2009. Assembly properties of the *Bacillus subtilis* actin, MreB. *Cell Motil. Cytoskeleton.* 66:109–118. http://dx.doi.org/10.1002/cm.20332

Miertzschke, M., C. Koerner, I.R. Vetter, D. Keilberg, E. Hot, S. Leonardy, L. Søgaard-Andersen, and A. Wittinghofer. 2011. Structural analysis of the Ras-like G protein MglA and its cognate GAP MglB and implications for bacterial polarity. *EMBO J.* 30:4185–4197. http://dx.doi.org/10.1038/emboj.2011.291

Mignot, T., J.W. Shaevitz, P.L. Hartzell, and D.R. Zusman. 2007. Evidence that focal adhesion complexes power bacterial gliding motility. *Science.* 315:853–856. http://dx.doi.org/10.1126/science.1137223

Nan, B., E.M. Mauriello, I.H. Sun, A. Wong, and D.R. Zusman. 2010. A multi-protein complex from *Myxococcus xanthus* required for bacterial gliding motility. *Mol. Microbiol.* 76:1539–1554. http://dx.doi.org/10.1111/j.1365-2958.2010.07184.x

Nan, B., J. Chen, J.C. Neu, R.M. Berry, G. Oster, and D.R. Zusman. 2011. Myxobacteria gliding motility requires cytoskeleton rotation powered by proton motive force. *Proc. Natl. Acad. Sci. USA.* 108:2498–2503. http://dx.doi.org/10.1073/pnas.1018556108

Nan, B., J.N. Bandaria, A. Moghtaderi, I.-H. Sun, A. Yildiz, and D.R. Zusman. 2013. Flagella stator homologs function as motors for myxobacterial gliding motility by moving in helical trajectories. *Proc. Natl. Acad. Sci. USA.* 110:E1508–E1513. http://dx.doi.org/10.1073/pnas.1219982110

Nan, B., J.N. Bandaria, K.Y. Guo, X. Fan, A. Moghtaderi, A. Yildiz, and D.R. Zusman. 2015. The polarity of myxobacterial gliding is regulated by direct interactions between the gliding motors and the Ras homolog MglA. *Proc. Natl. Acad. Sci. USA.* 112:E186–E193. http://dx.doi.org/10.1073/pnas.1421073112

Nurse, P., and K.J. Marians. 2013. Purification and characterization of *Escherichia coli* MreB protein. *J. Biol. Chem.* 288:3469–3475. http://dx.doi.org/10.1074/jbc.M112.413708

Patryn, J., K. Allen, K. Dziewanowska, R. Otto, and P.L. Hartzell. 2010. Localization of MglA, an essential gliding motility protein in *Myxococcus xanthus*. *Cytoskeleton (Hoboken).* 67:322–337.

Raftopoulou, M., and A. Hall. 2004. Cell migration: Rho GTPases lead the way. *Dev. Biol.* 265:23–32. http://dx.doi.org/10.1016/j.ydbio.2003.06.003

Rasmussen, R.K., J. Rusak, G. Price, P.J. Robinson, R.J. Simpson, and D.S. Dorow. 1998. Mixed-lineage kinase 2-SH3 domain binds dynamin and greatly enhances activation of GTPase by phospholipid. *Biochem. J.* 335:119–124.

Reimold, C., H.J. Defeu Soufo, F. Dempwolff, and P.L. Graumann. 2013. Motion of variable-length MreB filaments at the bacterial cell membrane influences cell morphology. *Mol. Biol. Cell.* 24:2340–2349. http://dx.doi.org/10.1091/mbc.E12-10-0728

Salje, J., F. van den Ent, P. de Boer, and J. Löwe. 2011. Direct membrane binding by bacterial actin MreB. *Mol. Cell.* 43:478–487. http://dx.doi.org/10.1016/j.molcel.2011.07.008

Sibley, L.D. 2010. How apicomplexan parasites move in and out of cells. *Curr. Opin. Biotechnol.* 21:592–598. http://dx.doi.org/10.1016/j.copbio.2010.05.009

Sun, M., M. Wartel, E. Cascales, J.W. Shaevitz, and T. Mignot. 2011. Motor-driven intracellular transport powers bacterial gliding motility. *Proc.*

Natl. Acad. Sci. USA. 108:7559–7564. http://dx.doi.org/10.1073/pnas.1101101108

Swulius, M.T., S. Chen, H. Jane Ding, Z. Li, A. Briegel, M. Pilhofer, E.I. Tocheva, S.R. Lybarger, T.L. Johnson, M. Sandkvist, and G.J. Jensen. 2011. Long helical filaments are not seen encircling cells in electron cryotomograms of rod-shaped bacteria. *Biochem. Biophys. Res. Commun.* 407:650–655. http://dx.doi.org/10.1016/j.bbrc.2011.03.062

Typas, A., M. Banzhaf, C.A. Gross, and W. Vollmer. 2012. From the regulation of peptidoglycan synthesis to bacterial growth and morphology. *Nat. Rev. Microbiol.* 10:123–136.

van den Ent, F., C.M. Johnson, L. Persons, P. de Boer, and J. Löwe. 2010. Bacterial actin MreB assembles in complex with cell shape protein RodZ. *EMBO J.* 29:1081–1090. http://dx.doi.org/10.1038/emboj.2010.9

van den Ent, F., T. Izoré, T.A. Bharat, C.M. Johnson, and J. Löwe. 2014. Bacterial actin MreB forms antiparallel double filaments. *eLife.* 3:e02634.

van Teeffelen, S., S. Wang, L. Furchtgott, K.C. Huang, N.S. Wingreen, J.W. Shaevitz, and Z. Gitai. 2011. The bacterial actin MreB rotates, and rotation depends on cell-wall assembly. *Proc. Natl. Acad. Sci. USA*. 108:15822–15827. http://dx.doi.org/10.1073/pnas.1108999108

Yang, R., S. Bartle, R. Otto, A. Stassinopoulos, M. Rogers, L. Plamann, and P. Hartzell. 2004. AglZ is a filament-forming coiled-coil protein required for adventurous gliding motility of *Myxococcus xanthus*. *J. Bacteriol.* 186:6168–6178. http://dx.doi.org/10.1128/JB.186.18.6168-6178.2004

Zhang, Y., M. Franco, A. Ducret, and T. Mignot. 2010. A bacterial Ras-like small GTP-binding protein and its cognate GAP establish a dynamic spatial polarity axis to control directed motility. *PLoS Biol.* 8:e1000430. http://dx.doi.org/10.1371/journal.pbio.1000430

Zhang, Y., A. Ducret, J. Shaevitz, and T. Mignot. 2012a. From individual cell motility to collective behaviors: insights from a prokaryote, *Myxococcus xanthus*. *FEMS Microbiol. Rev.* 36:149–164. http://dx.doi.org/10.1111/j.1574-6976.2011.00307.x

Zhang, Y., M. Guzzo, A. Ducret, Y.-Z. Li, and T. Mignot. 2012b. A dynamic response regulator protein modulates G-protein–dependent polarity in the bacterium *Myxococcus xanthus*. *PLoS Genet.* 8:e1002872. http://dx.doi.org/10.1371/journal.pgen.1002872